AGU PUBLICATIONS

Geophysical Research Letters

RESEARCH LETTER
10.1002/2014GL061307

Key Points:
- New methodology and large data set allowed detecting detailed atmospheric signal
- Atmospheric signal in InSAR time series contains systematic seasonal component
- Systematic correction is proposed that increases precision by a factor of 2

Correspondence to:
S. V. Samsonov,
sergey.samsonov@nrcan-rncan.gc.ca

Citation:
Samsonov, S. V., A. P. Trishchenko, K. Tiampo, P. J. González, Y. Zhang, and J. Fernández (2014), Removal of systematic seasonal atmospheric signal from interferometric synthetic aperture radar ground deformation time series, *Geophys. Res. Lett.*, *41*, 6123–6130, doi:10.1002/2014GL061307.

Received 23 JUL 2014
Accepted 18 AUG 2014
Accepted article online 23 AUG 2014
Published online 10 SEP 2014

Removal of systematic seasonal atmospheric signal from interferometric synthetic aperture radar ground deformation time series

Sergey V. Samsonov[1], Alexander P. Trishchenko[1], Kristy Tiampo[2], Pablo J. González[3], Yu Zhang[1], and José Fernández[4]

[1]Canada Centre for Mapping and Earth Observation, Natural Resources Canada, Ottawa, Ontario, Canada, [2]Department of Earth Sciences, Western University, London, Ontario, Canada, [3]Institute of Geophysics and Tectonics. School of Earth and Environment, University of Leeds, Leeds, UK, [4]Institute of Geosciences (CSIC-UCM), Madrid, Spain

Abstract Applying the Multidimensional Small Baseline Subset interferometric synthetic aperture radar algorithm to about 1500 Envisat and RADARSAT-2 interferograms spanning 2003–2013, we computed time series of ground deformation over Naples Bay Area in Italy. Two active volcanoes, Vesuvius and Campi Flegrei, are located in this area in close proximity to the densely populated city of Naples. For the first time, and with remarkable clarity, we observed decade-long elevation-dependent seasonal oscillations of the vertical displacement component with a peak-to-peak amplitude of up to 3.0 cm, substantially larger than the long-term deformation rate (<0.6 cm/yr). Analysis, utilizing surface weather and radiosonde data, linked observed oscillations with seasonal fluctuations of water vapor, air pressure, and temperature in the lower troposphere. The modeled correction is in a good agreement with observed results. The mean, absolute, and RMS differences are 0.014 cm, 0.073 cm, and 0.087 cm, respectively. Atmospherically corrected time series confirmed continuing subsidence at Vesuvius previously observed by geodetic techniques.

1. Introduction

Interferometric synthetic aperture radar (InSAR) is an established technique for retrieval of ground deformation from synthetic aperture radar (SAR) data [*Massonnet and Feigl*, 1998; *Rosen et al.*, 2000]. Processing of multitemporal InSAR imagery produces time series of ground deformation for events occurring over an extended period of time [*Berardino et al.*, 2002; *Hooper*, 2008; *Samsonov and d'Oreye*, 2012]. InSAR retrievals are contaminated by the atmospheric signal, called the Atmospheric Path Delay (APD), at a magnitude often exceeding the deformation signal itself [*Wadge et al.*, 2002; *Heleno et al.*, 2010]. A precise atmospheric correction, applied to individual interferograms, requires an accurate knowledge of temporally and spatially colocated atmospheric profiles, which are not always easily available. The Global Positioning System (GPS), remote sensing retrievals, meteorological, or weather models can produce atmospheric profiles, but their accuracy, spatial details, and temporal collocation with InSAR images are often insufficient for achieving satisfactory results [*Fournier et al.*, 2011].

Delacourt et al. [1998] calculated an atmospheric correction from surface measurements of meteorological parameters and applied it to 20 ERS interferograms over Mount Etna. This study showed that atmospheric signal in the individual interferograms can be as high as 6 ± 3 cm. However, it was limited to a 1 year period, making it difficult to reliably evaluate the true rate of ground deformation. The *Wadge et al.* [2002] correction for one ERS interferogram over Mount Etna was computed from GPS data, which lacks detailed spatial resolution.

Li et al. [2005] estimated atmospheric correction from GPS and Moderate Resolution Imaging Spectroradiometer (MODIS) data and applied it to three interferograms over southern California. MODIS data can only be used during the day and with no cloud cover. The *Fournier et al.* [2011] correction, derived from ERA-40 weather model, was applied to 136 interferograms (combined into two stacks) over the South America western coast. They found that due to poor temporal and spatial resolution of the weather model data, their atmospheric correction failed to produce reliable results. Among other things, they recommended improving empirical corrections constrained by real atmospheric data in conjunction with deformation models. The *Jolivet et al.* [2011] correction, based on the ERA-I weather model, was applied to 35 Envisat interferograms

©2014. Her Majesty the Queen in Right of Canada.

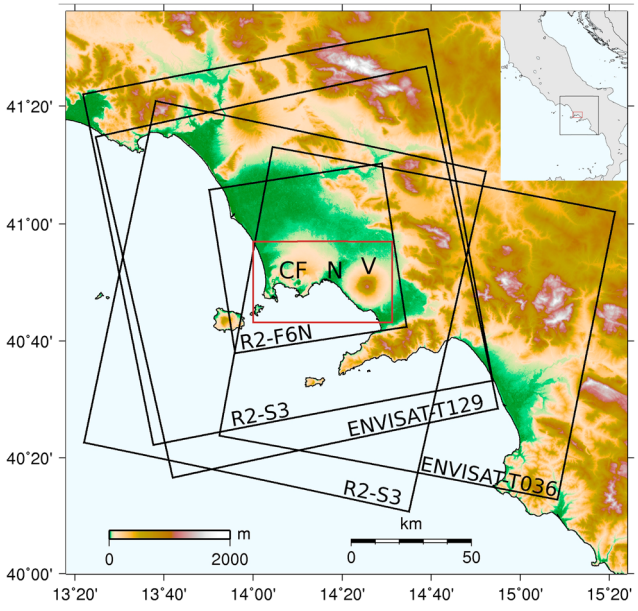

Figure 1. Naples Bay Area in Italy (see extent in top right corner). SAR frames (in black): Envisat ascending track 129, descending track 036, and RADARSAT-2 ascending tracks Fine-6 Near (F6N) and Standard-3 (S3) and descending Standard-3 (S3). Region of interest (in brown) covers Campi Flegrei (CF), Vesuvius (V), and City of Naples (N). Background is 30 m ASTER DEM.

acquired over the Tibetan Plateau during the 2003 to 2010 period. Although the authors clearly demonstrated the importance of atmospheric path delay correction to reduce the risk of unwrapping errors, the derivation of the ground deformation rates was not obvious from their results.

In 2003–2013 ground deformation time series, computed from 1457 Envisat and RADARSAT-2 interferograms acquired over Naples Bay area in Italy, we observed periodic oscillations with an elevation-dependent peak-to-peak amplitude greater than 3.0 cm superimposed on a long-term deformation trend <0.6 cm/yr. Previous studies identified this area as one of the most endangered on Earth due to its proximity to the Vesuvius and Campi Flegrei active volcanoes [*Borgia et al.*, 2005]. The vertical and horizontal time series were computed with the advanced Multidimensional Small Baseline Subset (MSBAS) technique [*Samsonov and d'Oreye*, 2012; *Samsonov et al.*, 2014] that combined data from three ascending and two descending multisensor beams into a set of high temporal resolution and high precision time series. Altogether, 250 scenes were processed over the 10 year period, an average of approximately one image every 2 weeks. This temporal frequency and a decade-long time span of data set enables us to resolve in unprecedented detail the atmospheric seasonal oscillations mapped onto the ground deformation time series.

The systematic component of the atmospheric signal that we identified and, for the first time, extracted from the multitemporal time series accounts for nearly half of the total noise computed with respect to a linear trend. This systematic component cannot be filtered out or eliminated by averaging multiple interferograms without significantly affecting the deformation signal. Understanding the temporal variability and elevation dependence of APD allows for the development of a methodology for calculating systematic atmospheric correction in multitemporal InSAR ground deformation retrievals.

2. Data Processing

Ground deformation time series were computed from Envisat and RADARSAT-2 SAR data acquired between 5 June 2003 and 16 February 2013 when both ascending and descending images were available (Figure 1 and Table 1). InSAR analysis was performed with GAMMA software [*Wegmuller and Werner*, 1997] and the topographic phase was computed from the Advanced Spaceborne Thermal Emission and Reflection Radiometer (ASTER) 30 m digital elevation model (DEM) (from U.S. Geological Survey Global Explorer, http://gdex.cr.usgs.gov/gdex/). Interferograms were spatially filtered [*Goldstein and Werner*, 1998], unwrapped [*Costantini*, 1998], and detrended using the baseline correction algorithm implemented in GAMMA. All possible interferograms were computed but only highly coherent interferograms (average coherence after filtering >0.6) were resampled to a reduced resolution 40 × 40 m grid and used for time series analysis.

The MSBAS technique was applied to produce vertical and horizontal time series of ground deformation over the 10 year period. In this study only the vertical component of the time series is discussed. The MSBAS technique employs the Singular Value Decomposition for solving for two-dimensional deformation time series and residual topographic error. It is capable of simultaneously processing InSAR data from multiple sensors with different acquisition geometry, wavelength (i.e., X, C, and L bands), resolution, and coverage. During MSBAS processing the deformation time series were regularized [*Tikhonov and Arsenin*, 1977]. Var-

©2014. Her Majesty the Queen in Right of Canada.

Table 1. Envisat and RADARSAT-2 Synthetic Aperture Radar Data Used in This Study: θ is Azimuth and ϕ Is Incidence Angle, N Is Number of Images, and M Is Number of Interferograms Computed for Each Data Set[a]

InSAR Set	Orbit	UTM	Coverage	θ°	ϕ°	N	M
Envisat, Track 129	asc	20:47	20021113-20091216	344.0	22.8	55	276
Envisat, Track 036	dsc	09:20	20030605-20101021	195.9	22.8	58	196
RADARSAT-2, S3	asc	16:57	20090119-20130215	348.7	35.1	39	156
RADARSAT-2, S3	dsc	05:10	20081227-20130216	190.4	35.1	50	422
RADARSAT-2, F6	asc	17:09	20081229-20121208	351.0	48.3	48	407
Total:			20030605-20130215			250	1457

[a]asc, ascending; dsc, descending; UT, universal time.

ious regularization parameters in the range 0.05–1 were tested and 0.25 was selected using the "L curve" methodology [*Hansen and O'Leary*, 1993]. Time series were referenced to a point located in the downtown of Naples, close to the Napoli/Capodichino weather station (40.85°N, 14.30°E, elevation 72 m). A linear deformation rate shown in Figure 2 (left) was calculated by fitting a straight line to the vertical component of the time series. Uplift at Campi Flegrei and subsidence at Vesuvius are clearly observed in these results.

Coarser resolution time series were computed for a 5 × 5 pixel (200 × 200 m) grid for the entire region. Spatial averaging was performed in order to reduce the number of time series and to increase the signal-to-noise ratio. Pronounced annual oscillations are observed in the vertical component of time series superimposed on the long-term deformation trend, such as subsidence at the summit of Vesuvius (Figure 2, right). The peak-to-peak amplitude of the oscillations can be as high as 3.0 cm and is proportional to elevation, which ranges from 0 m at the coast to about 1000 m at Vesuvius's summit. The maximum oscillations occur in the summer and the minimum occurs in the winter. Larger than average displacement (apparent uplift) observed during summer of 2011 is due to reversible ground deformation that occurred in the south west flank of Vesuvius. This motion lasted approximately 6 months (i.e., 3 months of subsidence followed by 3 months of uplift) and is clearly observed in the individual interferograms derived from multiple SAR images and is also detected by the daily GPS observations during the entire period, as reported by *Tammaro et al.* [2013, Figure 2]. It is worth noting that InSAR time series capture apparent range change between the point of measurement and the reference point, rather than actual ground displacements.

3. Seasonal Atmospheric Signal

InSAR retrievals are detached from an external reference frame (i.e., WGS84 or ITRF2000). They are derived by subtracting a value observed at the chosen stable reference point from the values of displacements

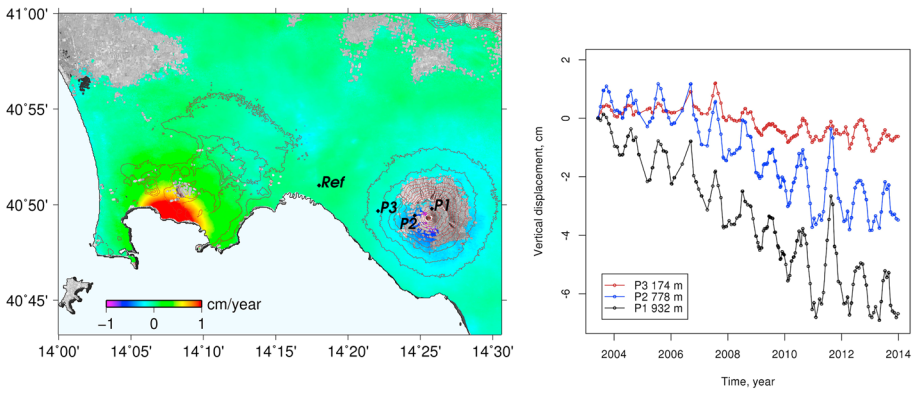

Figure 2. (left) Vertical displacement rate from Envisat and RADARSAT-2 data acquired during 2003–2013 period. Background is RADARSAT-2 F6N image. Shown in brown are 100 m topographic contour lines. Reference region is marked as "Ref" and measurement points are marked as P1–P3. For visualization displacement rate values were limited to [−1; 1]. (right) Time series of vertical deformation measured at points P1–P3 located on flanks of Vesuvius at heights 174, 778, and 932 m correspondingly.

©2014. Her Majesty the Queen in Right of Canada.

produced for each pixel in the interferogram. Such one-way line of sight (LOS) range change $\Delta\rho_{\mathrm{obs},i}$ at a point i is a difference of range changes measured at a point i at elevation z_i and a reference point at elevation z_r:

$$\Delta\rho_{\mathrm{obs},i} = \Delta\rho_i - \Delta\rho_r = (\rho(t_m, z_i) - \rho(t_s, z_i)) - (\rho(t_m, z_r) - \rho(t_s, z_r)), \quad (1)$$

where $\rho(t, z)$ is a LOS range as a function of acquisition time and elevation and t_m and t_s are master (i.e., reference image) and slave image acquisition times. It is assumed that $t_m < t_s$ so the positive values of $\Delta\rho_{\mathrm{obs},i}$ correspond to range shortening (apparent uplift).

Assuming that residual orbital, decorrelation, and thermal components are negligibly small, the observed signal consists of two components, due to ground deformation and the atmospheric path delay $\rho = \rho^{\mathrm{def}} + \rho^{\mathrm{apd}}$. Substituting this equation into (1) allows explicit representation of the deformation and atmospheric components:

$$\begin{aligned}\Delta\rho_{\mathrm{obs},i} &= (\rho^{\mathrm{def}}(t_m, z_i) - \rho^{\mathrm{def}}(t_s, z_i)) - (\rho^{\mathrm{def}}(t_m, z_r) - \rho^{\mathrm{def}}(t_s, z_r)) \\ &\quad + (\rho^{\mathrm{apd}}(t_m, z_i) - \rho^{\mathrm{apd}}(t_m, z_r)) - (\rho^{\mathrm{apd}}(t_s, z_i) - \rho^{\mathrm{apd}}(t_s, z_r)) \\ &= \Delta\rho_i^{\mathrm{def}}(t_m, t_s) + \Delta\rho^{\mathrm{apd}}(t_m, t_s, z_r, z_i). \end{aligned} \quad (2)$$

Here the first four terms were combined into the deformation component $\Delta\rho_i^{\mathrm{def}}(t_m, t_s)$ for each pixel i and the remaining four terms were combined into the APD component $\Delta\rho^{\mathrm{apd}}(t_m, t_s, z_r, z_i)$, which is elevation dependant.

The atmospheric signal in InSAR interferograms consists of ionospheric and tropospheric components [*Gray et al.*, 2000; *Meyer et al.*, 2006]. The magnitude of the differential (i.e., between master and slave acquisitions) ionospheric signal in case of X and C band InSAR is insignificant and elevation independent, and is not considered here. The tropospheric signal includes hydrostatic (dry air) and wet components [e.g., *Martin and Waldron*, 1961; *Hurter and Maier*, 2013]. While the hydrostatic component is larger than the wet component, its seasonal fluctuations are significantly smaller [*Bevis et al.*, 1992; *Zebker et al.*, 1997]. Atmospheric path delay in SAR data is calculated by integrating refractivity along the radar wave path, which can be estimated from atmospheric parameters, such as air temperature, atmospheric, and water vapor pressures [*Delacourt et al.*, 1998; *Hofmann-Wellenhof et al.*, 2001]. These parameters can be measured at the Earth's surface by a weather station, at altitude by radiosonde, or derived from weather models, GPS, or remote sensing retrievals [*Lowry et al.*, 2002; *Hurter and Maier*, 2013]. The InSAR ground deformation retrieval technique is affected by the difference between master and slave APDs, and as we show later, the temporal variability of refractivity is more important than its absolute value, because of a strong repeatable seasonal cycle.

Assuming vertical 1-D model, the atmospheric component $\Delta\rho_i^{\mathrm{apd}}$ can be computed by integrating refractivity $N = 10^6(n-1)$ in the range of elevations between the reference and measurement points, where $n = \frac{c}{v}$ is the refractive index, c is the speed of light in vacuum, and v is the speed of light in the atmosphere [e.g., *Martin and Waldron*, 1961; *Hofmann-Wellenhof et al.*, 2001].

$$\Delta\rho_i^{\mathrm{apd}}(t_m, t_s, z_r, z_i) = 10^{-6}\int_{z_r}^{z_i} \Delta N(t_m, t_s, z)\mathrm{d}z: \quad (3)$$

where $\Delta N(t_m, t_s, z) = N(t_m, z) - N(t_s, z)$ is a difference of refractivities at times t_m and t_s at elevation z.

Because the vertical component of deformation time series is used here, in (3) normalization by the SAR incidence angle is not required.

In case of the exponential decay model [*Martin and Waldron*, 1961], the refractivity at arbitrary elevation is a product of the time-dependent term measured at the Earth's surface N_{z_r} and the exponential vertical profile factor e^{-cz}. The atmospheric path delay in such a case can be computed analytically by integration of the decay function:

$$\Delta\rho_i^{\mathrm{apd}}(t_m, t_s, z_r, z_i) = 10^{-6}\Delta N_{z_r}(t_m, t_s)\int_{z_r}^{z_i} e^{-cz}\mathrm{d}z. \quad (4)$$

The exponential decay single-parameter model is selected due to its simplicity but the multiparametric Hopfield model [*Hopfield*, 1969] produces similar results. Refractivity computed from radiosonde measurements of temperature, air, and water vapor (computed from the dew point temperature according

©2014. Her Majesty the Queen in Right of Canada.

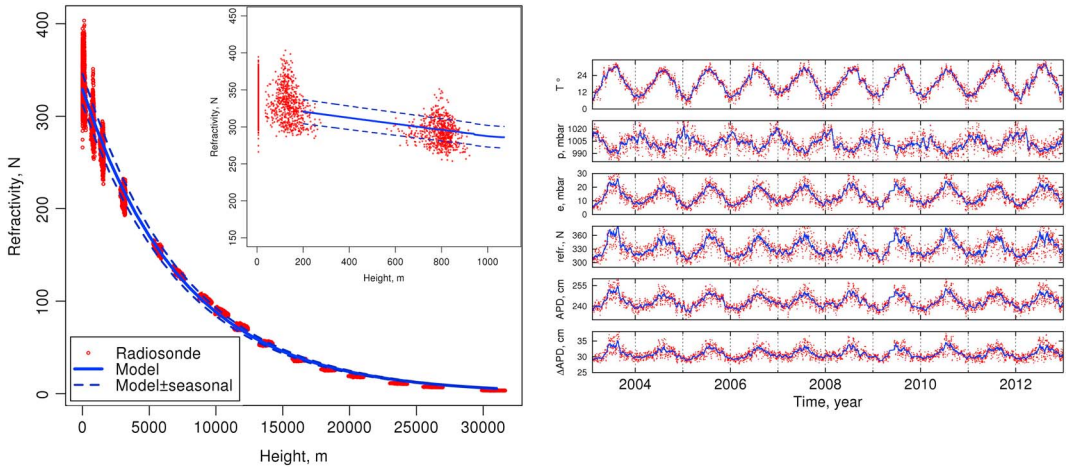

Figure 3. (left) Refractivity as function of height computed from radiosonde measurements of temperature, atmospheric, and water pressures (in red) observed twice daily during 2012. Fitted mean and seasonal fluctuation of exponential model (in blue). Radiosonde data were acquired by Pratica di Mare weather station located near Rome, Italy. Insert shows same data at 0–1000 m elevations. (right) Parameters measured at weather station Napoli/Capodichino approximately colocated with Ref point from 2 (left): temperature (T), atmospheric pressure (p), water vapor pressure (e), and computed parameters: refractivity (refr.) at Earth's surface, atmospheric path delay (APD) at the Earth's surface, and fraction of APD (ΔAPD) accumulated between reference and measurement points with elevation difference of 1000 m. A 20 day average is plotted in blue.

to *Alduchov and Eskridge* [1996]) pressures performed during a 1 year period twice daily at the Pratica di Mare (about 200 km north of Naples) is shown in Figure 3 (left). The fitted exponential model with the decay parameter $c = 0.132\,\mathrm{km}^{-1}$ and refractivity at the Earth's surface (mean value ± seasonal amplitude) $N = 329 \pm 17$ N-units is also shown. If the fit is applied only to data points within the lowest 1 km layer, then $c = 0.165\,\mathrm{km}^{-1}$ and $N = 334$ N-units. Such a small value of c essentially means the linear growth of APD in the lowest 1 km atmospheric layer with a scale factor $1/c$ being equal to 5.9 km. While the available radiosonde data spanned 10 year period, we found that 1 year subset is sufficient for an accurate model fitting. Standard deviation of these modeled parameters is equal to 3 N-units, and 0.001 km^{-1} for the entire elevation range and 4 N-units, and 0.008 km^{-1} for the lowest 1 km atmospheric layer.

The amplitude of refractivity at the Earth's surface was estimated by fitting the sine function to the smoothed refractivity time series computed from meteorological observations at the weather station Napoli/Capodichino, located in close proximity to the reference point. The seasonal pattern in all parameters is clearly visible, with temperature and water vapor pressure reaching their maximum during summer and atmospheric pressure reaching its maximum during winter (Figure 3, right).

The amplitude of the seasonal APD oscillation in the multitemporal MSBAS InSAR deformation time series can be analytically computed as a function of elevation:

$$\Delta\overline{\rho^{\mathrm{apd}}(z_r, z_i)} = 10^{-6}\overline{\Delta N_{z_r}} \int_{z_r}^{z_i} e^{-cz}\mathrm{d}z = \frac{10^{-6}\overline{\Delta N_{z_r}}}{ce^{cz_r}}(1 - e^{-c(z_i - z_r)}), \tag{5}$$

where an overbar means the average seasonal amplitude, i.e., $\overline{\rho^{\mathrm{apd}}(z_r, z_i)}$ is the average seasonal amplitude of APD observed in a vertical component of ground deformation time series, and $\overline{\Delta N_{z_r}}$ is the average seasonal amplitude of refractivity at the Earth's surface.

It also can be estimated from the InSAR time series by simultaneously fitting the sine and linear functions to the vertical component of MSBAS InSAR time series for all points on the map:

$$\Delta\rho_{\mathrm{obs},i}(t_m, t_s, z_r, z_i) = at + b + \overline{\Delta\rho^{\mathrm{apd}}(z_r, z_i)}\sin\left(\frac{2\pi t}{T} + \phi_0\right), \tag{6}$$

where a and b are parameters describing linear trend, T is a period of oscillations equal to 1 year, and ϕ_0 is a phase offset. Due to lower signal-to-noise ratio for APD at small elevations, the fitting of ϕ_0 was found to produce a noisy result. This value was derived from higher elevation results and used for all elevations as a

©2014. Her Majesty the Queen in Right of Canada.

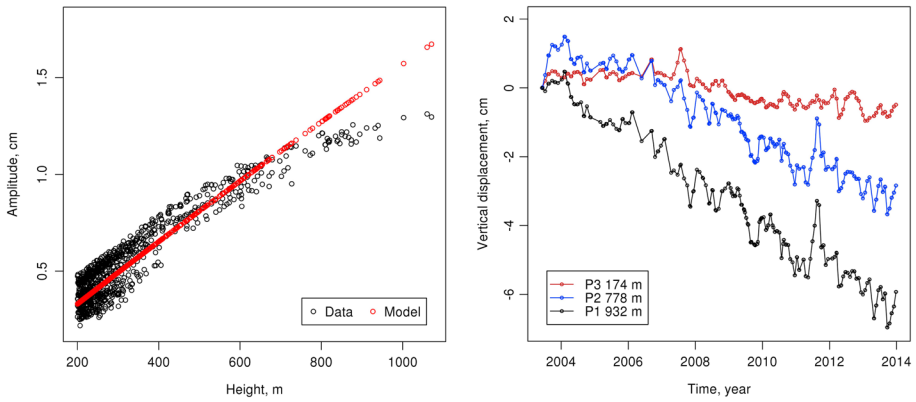

Figure 4. (left) Amplitude of seasonal oscillations observed in the vertical component of deformation time series as function of height (in black). Amplitude based on exponential decay model with parameters derived from radiosonde measurement (in red). (right) Same as in Figure 2 (right), time series of vertical deformation after applying atmospheric correction.

constant rather than a fitting parameter. It is equal to a 7.7 month shift from the beginning of the calendar year, which leads to the maximum of APD during the summer, as shown at the bottom in Figure 3 (right). Here we assume that true ground deformation is a linear function of time, and variations from this line are caused by seasonal variability of atmospheric path delay. Altogether, on a map shown in Figure 2 (left) we found a large number (i.e., 879) of good points located at elevations above 200 m and suitable for fitting a model (6).

The amplitude of the seasonal oscillation in multitemporal InSAR ground deformation time series as a function of elevation is plotted in Figure 4 (left). The exponential model from Figure 3 (left) computed from radiosonde and weather station observation also is shown in Figure 4 (left). As noted earlier, for this range of elevations, the exponential model is effectively reduced to a linear one. There is good overall agreement between the two annual amplitudes of atmospheric path delay derived from (5) and (6). The mean, absolute, and RMS differences are 0.014 cm, 0.073 cm, and 0.087 cm, respectively. The deviation between modeled and observed values at elevations above 700 m is also apparent. It cannot be unambiguously explained. Spatial filtering applied to the interferogram during InSAR analysis prior to phase unwrapping could be a possible cause. This could be validated in regions without stratovolcano topography. Another possible reason could be the use of the sine function, which may not reproduce the peak values precisely and therefore reduces the amplitude of the seasonal cycle.

An APD correction based on the exponential decay model with refractivity at the surface changing according to a sine function was integrated into the MSBAS InSAR processing. Corrected time series are shown in Figure 4 (right) for the same points as in Figure 2 (left). The average RMS error, assuming linear trend deformation model, decreased from 0.40 to 0.29 cm (30%) for the entire region and from 0.63 to 0.37 cm (41%) for points at elevation greater than 500 m. The actual precision improvement is likely higher than 50%, which can be validated by comparing MSBAS time series with independent measurements from GPS or leveling that are not freely available for this region. The remaining noise can be in part caused by imprecise estimation of incidence angles, which are assumed to be constant throughout interferograms (which significantly reduces processing time) and also due to neglecting the north-south component of deformation, which is not well resolved by the spaceborne InSAR and accounts for about 5% of the total signal. This could also be due to the deviation between model and InSAR observations at elevations above 700 m and amplitude varying seasonal oscillation that is not perfectly captured by the constant amplitude sine function fit.

4. Discussion and Conclusions

The large amount of SAR data available for this study and the state-of-the-art processing methodology allowed the detection of seasonal variations of the atmospheric path delay with clarity that has not been reported before. Almost 1500 hundred interferograms were generated from 250 SAR images over the 2003–2013 period, for time steps of approximately 2 weeks. This high-density temporal resolution enabled resolution of the seasonal cycle very well. The peak-to-peak annual amplitude of variations in the vertical

©2014. Her Majesty the Queen in Right of Canada.

component of the deformation time series observed at Vesuvius (elevation 1281 m) during the 2003–2013 period reaches 3 cm while the long-term subsidence rate is less than 0.6 cm/yr. Seasonal oscillations of APD larger amplitudes occur at other stratovolcanoes, in particularly at Pico do Fogo (2829 m), Mount Etna (3350 m), and Mount Cameroon (4040 m), as was demonstrated by *Wadge et al.* [2002] and *Heleno et al.* [2010]. Proposed here approach can be successfully used for correcting InSAR retrievals in those and other areas.

For an accurate measurement of the deformation rate, particularly from multitemporal InSAR data spanning a short period of time, the removal of atmospheric oscillations is critical. The atmospheric correction model was designed in this study based on multiyear statistics of atmospheric refractivity calculated from meteorological and radiosonde observations available for this region. It is generally in good agreement with the observed seasonal cycle of atmospheric signal deduced from the InSAR deformation time series. It successfully removes the systematic component of APD from multitemporal InSAR time series, which accounts for about half of the total phase variability. Deviation of the observed amplitude at elevations higher than 700 m from predictions based on the exponential decay model is an interesting fact and requires further investigation. Continuing subsidence at Vesuvius previously observed by geodetic techniques is confirmed here with the atmospherically corrected InSAR retrievals. The impact of systematic atmospheric path delay is significantly reduced in the refined deformation rate maps and deformation time series.

Acknowledgments

We thank CSA for providing RADARSAT-2 and ESA for providing Envisat data under project 12984. Radiosonde data were acquired at Pratica di Mare weather station located near Rome, Italy, and provided by British Atmospheric Data Centre. Climate data were provided by NOAA National Climatic Data Center. Postprocessing was performed and figures were plotted with R, GMT, and GNUPLOT software. K.F.T. was supported by an NSERC Discovery grant. This research also was supported by MINECO research project AYA2010-17448 and MED-SUV project from the EU Seventh Programme for research, technological development, and demonstration under agreement 308665. It is a contribution for the Moncloa Campus of International Excellence. Value-added products derived from Envisat and RADARSAT-2 data as well as deformation time series and deformation rate maps computed with the MSBAS technique will be provided by the corresponding author upon request. We would like to thank reviewers Zhen Liu and Sandra Heleno for their valuable comments.

The Editor thanks Zhen Liu, Sandra Heleno, and an anonymous reviewer for their assistance in evaluating this paper.

References

Alduchov, O., and R. Eskridge (1996), Improved Magnus form approximation of saturation vapor pressure, *J. Appl. Meteorol.*, *35*, 601–609.

Berardino, P., G. Fornaro, and R. Lanari (2002), A new algorithm for surface deformation monitoring based on small baseline differential SAR interferograms, *IEEE Trans. Geosci. Remote Sens.*, *40*(11), 2375–2383.

Bevis, M., S. Businger, T. Herring, C. Rocken, R. Anthes, and R. Ware (1992), GPS meteorology: Remote sensing of atmospheric water vapor using the global positioning system, *J. Geophys. Res.*, *97*(D14), 15,787–15,801, doi:10.1029/92JD01517.

Borgia, A., et al. (2005), Volcanic spreading of Vesuvius, a new paradigm for interpreting its volcanic activity, *Geophys. Res. Lett.*, *32*, L03303, doi:10.1029/2004GL022155.

Costantini, M. (1998), A novel phase unwrapping method based on network programming, *IEEE Trans. Geosci. Remote Sens.*, *36*(3), 813–821.

Delacourt, C., P. Briole, and J. Achache (1998), Tropospheric corrections of SAR interferograms with strong topography. Application to Etna, *Geophys. Res. Lett.*, *25*(15), 2849–2852, doi:10.1029/98GL02112.

Fournier, T., M. Pritchard, and N. Finnegan (2011), Accounting for atmospheric delays in InSAR data in a search for long-wavelength deformation in South America, *IEEE Trans. Geosci. Remote Sens.*, *49*(10), 3856–3867, doi:10.1109/TGRS.2011.2139217.

Goldstein, R., and C. Werner (1998), Radar interferogram filtering for geophysical applications, *Geophys. Res. Lett.*, *25*(21), 4035–4038.

Gray, L., K. Mattar, and G. Sofko (2000), Influence of ionospheric electron density fluctuations on satellite radar interferometry, *Geophys. Res. Lett.*, *27*(10), 1451–1454.

Hansen, P., and D. O'Leary (1993), The use of the L-curve in the regularization of discrete ill-posed problems, *SIAM J. Sci. Comput.*, *14*(6), 1487–1503.

Heleno, S., C. Frischknecht, N. d'Oreye, J. Lima, B. Faria, R. Wall, and F. Kervyn (2010), Seasonal tropospheric influence on SAR interferograms near the ITCZ the case of Fogo Volcano and Mount Cameroon, *J. Afr. Earth. Sci.*, *58*(5), 833–856, doi:10.1016/j.jafrearsci.2009.07.013.

Hofmann-Wellenhof, B., H. Lichtenegger, and J. Collins (2001), *GPS Theory and Practice*, 326 pp., Springer, Vienna, Austria.

Hooper, A. (2008), A multi-temporal InSAR method incorporating both persistent scatterer and small baseline approaches, *Geophys. Res. Lett.*, *35*, L16302, doi:10.1029/2008GL034654.

Hopfield, H. S. (1969), Two-quartic tropospheric refractivity profile for correcting satellite data, *J. Geophys. Res.*, *74*(18), 4487–4499, doi:10.1029/JC074i018p04487.

Hurter, F., and O. Maier (2013), Tropospheric profiles of wet refractivity and humidity from the combination of remote sensing datasets and measurements on the ground, *Atmos. Meas. Tech. Discuss.*, *6*, 4895–4940, doi:10.5194/amtd-6-4895-2013.

Jolivet, R., R. Grandin, C. Lasserre, M. Doin, and G. Peltzer (2011), Systematic InSAR tropospheric phase delay corrections from global meteorological reanalysis data, *Geophys. Res. Lett.*, *38*, L17311, doi:10.1029/2011GL048757.

Li, Z., J.-P. Muller, P. Cross, and E. J. Fielding (2005), Interferometric synthetic aperture radar (InSAR) atmospheric correction: GPS, Moderate Resolution Imaging Spectroradiometer (MODIS), and InSAR integration, *J. Geophys. Res.*, *110*, B03410, doi:10.1029/2004JB003446.

Lowry, A. R., C. Rocken, S. V. Sokolovskiy, and K. D. Anderson (2002), Vertical profiling of atmospheric refractivity from ground-based GPS, *Radio Sci.*, *37*(3), 13–1–13–19, doi:10.1029/2000RS002565.

Martin, F., and C. Waldron (1961), A layered exponential model of radar refractivity, *J. Geophys. Res.*, *66*(12), 4129–4135, doi:10.1029/JZ066i012p04129.

Massonnet, D., and K. Feigl (1998), Radar interferometry and its application to changes in the Earth's surface, *Rev. Geophys.*, *36*(4), 441–500.

Meyer, F., R. Bamler, N. Jakowski, and T. Fritz (2006), The potential of low-frequency SAR systems for mapping ionospheric TEC distributions, *IEEE Geosci. Remote Sens. Lett.*, *3*(4), 560–564.

Rosen, P., P. Hensley, I. Joughin, F. Li, S. Madsen, E. Rodriguez, and R. Goldstein (2000), Synthetic aperture radar interferometry, *Proc. IEEE*, *88*(3), 333–382.

Samsonov, S., and N. d'Oreye (2012), Multidimensional time series analysis of ground deformation from multiple InSAR data sets applied to Virunga Volcanic Province, *Geophys. J. Int.*, *191*(3), 1095–1108, doi:10.1111/j.1365-246X.2012.05669.x.

Samsonov, S., N. d'Oreye, P. González, K. Tiampo, L. Ertolahti, and J. Clague (2014), Rapidly accelerating subsidence in the Greater Vancouver region from two decades of ERS-ENVISAT-RADARSAT-2 DInSAR measurements, *Remote Sens. Environ.*, *143*, 180–191, doi:10.1016/j.rse.2013.12.017.

©2014. Her Majesty the Queen in Right of Canada.

Tammaro, U., P. De Martino, F. Obrizzo, G. Brandi, A. D'Alessandro, M. Dolce, S. Malaspina, C. Serio, and F. Pingue (2013), Somma Vesuvius volcano: Ground deformations from CGPS observations (2001–2012), *Ann. Geophys.*, *56*(4), S0456, doi:10.4401/ag-6462.

Tikhonov, A., and V. Arsenin (1977), *Solution of Ill-Posed Problems*, Winston and Sons, Washington, D. C.

Wadge, G., et al. (2002), Atmospheric models, GPS and InSAR measurements of the tropospheric water vapour field over Mount Etna, *Geophys. Res. Lett.*, *29*(19), 1905, doi:10.1029/2002GL015159.

Wegmuller, U., and C. Werner (1997), Gamma SAR processor and interferometry software, *The 3rd ERS Symposium on Space at the Service of our Environment,* Florence, Italy. [Available at http://earth.esa.int/workshops/ers97/papers/wegmuller2/.]

Zebker, H., P. Rosen, and S. Hensley (1997), Atmospheric effects in interferometric synthetic aperture radar surface deformation and topographic maps, *J. Geophys. Res.*, *102*(B4), 7547–7563, doi:10.1029/96JB03804.

©2014. Her Majesty the Queen in Right of Canada.